COMPARATIVE STUDY OF MICROSTRUCTURAL AND MAGNETIC PROPERTIES OF IN-SITU AND BALL MILLED SYNTHESIZED LSMO: COBALT FERRITE NANOCOMPOSITES USING MICROWAVE OVEN

A THESIS SUBMITTED IN PARTIAL FULFILLMENT
OF THE REQUIREMENTS FOR THE DEGREE OF

Master of Technology
In
Metallurgical and Materials Engineering

By
BISHNUPRIYA BEHERA
Roll No- 209MM1235

Department of Metallurgical and Materials Engineering
National Institute of Technology
Rourkela
2011

COMPARATIVE STUDY OF MICROSTRUCTURAL AND MAGNETIC PROPERTIES OF IN-SITU AND BALL MILLED SYNTHESIZED LSMO: COBALT FERRITE NANOCOMPOSITES USING MICROWAVE OVEN

A THESIS SUBMITTED IN PARTIAL FULFILLMENT
OF THE REQUIREMENTS FOR THE DEGREE OF

Master of Technology
In
Metallurgical and Materials Engineering

By
BISHNUPRIYA BEHERA
Roll No- 209MM1235

Under the Guidance of
Prof. D. Chaira and Prof. Bibhuti B. Nayak

Department of Metallurgical and Materials Engineering
National Institute of Technology
Rourkela
2011

National Institute of Technology

Rourkela

CERTIFICATE

This is to certify that this thesis entitled, "**Microstructural and magnetic properties of in-situ and ball mill synthesized LSMO: $CoFe_2O_4$ nanocomposites using microwave oven**" submitted by **Bishnupriya Behera** in partial fulfillments for the requirements for the award of Master of Technology Degree in Metallurgical and Materials Engineering at National Institute of Technology, Rourkela is an authentic work carried out by her under our guidance.

To the best of my knowledge, the matter embodied in the thesis has not been submitted to any other University / Institute for the award of any Degree or Diploma.

Prof. D. Chaira
Assistant Professor
Department of Metallurgical and Materials Engineering
National Institute of Technology
Rourkela- 769 008

Prof. Bibhuti B. Nayak
Associate Professor
Department of Ceramic Engineering
National Institute of Technology
Rourkela- 769 008

ACKNOWLEDGEMENTS

With deep regards and profound respect, I avail this opportunity to express my deep sense of gratitude and indebtedness to Prof. D. Chaira, Department of Metallurgical and Materials Engineering Engineering and Prof. Bibhuti B. Nayak, Department of Ceramic Engineering, NIT Rourkela, for introducing the present research topic and for his inspiring guidance, constructive criticism and valuable suggestion throughout in this research work. It would have not been possible for me to bring out this thesis without their help and constant encouragement.

I am sincerely thankful to Prof. B. B. Verma, Head, Department of Metallurgical and Materials Engineering, for his advice and providing necessary facility for my work.

I would also like to thank Prof. S. K. Pratihar, Department of Ceramics Engineering, NIT Rourkela, for helping and carrying out different characterization**.**

Special thanks to Subrat Mohanty, Geetanjali Parida, Arpita Das and Pankajini Sahani, as a PhD Scholars of the department for being so supportive and helpful in every possible way.

I am highly grateful to all staff members of Department of Metallurgical and Materials Engineering and Ceramic Engineering, N.I.T., Rourkela, for their help during the execution of experiments.

Last but not the least, Special thanks to my husband Mr. Sujit kumar Tahal, family members, parents and friends for being so supportive and helpful in every possible way.

June, 2011 **Bishnupriya Behera**

CONTENTS

Abstract

Manganite-ferrite nanocomposites are of interest due to the magnetic coupling between these two phases that affects the microstructural and magnetic properties. These composite materials are of enormous technological importance, as these materials can be used as read heads for hard disks, magnetic storage and sensing devices. In this work, microwave assisted synthesis was carried out for the preparation of (1-x) mol % $La_{0.67}Sr_{0.33}MnO_3$ (LSMO): x mol % $CoFe_2O_4$ (CF) (where x= 0, 30, 50, 70 and 100) nanopowders and nanocomposites by using microwave oven. The main objectives of this work are: (i) study the effect of CF addition on the microstructural and magnetic properties of LSMO: CF composites. (ii) Comparative study of microstructural and magnetic properties of in-situ and ball milled synthesized LSMO: cobalt ferrite nanocomposites using microwave oven. Different characterization techniques such as DSC-TG, XRD, particle size analysis, SEM, density and M-H loop have been performed to study the properties of these composites.

Minimum calcinations temperature for pure LSMO and CF powders is 800 °C as observed from thermal analysis. X-ray diffraction analysis confirms the presence of two phases with either LSMO or CF, without any impurities. The most intense peak of LSMO in ball-milled synthesized LSMO: CF composites show more strain due to its high density microstructure and small size with nearly spherical in shape as compared to in-situ LSMO: CF composites. The particle size of LSMO is smaller as compared to CF in these composites. Back-scattered SEM with EDAX confirms the two phase system of all LSMO: CF composites except for 70 mol% LSMO: 30 mol% CF ball-milled composites (thin layer of CF is well surrounded on LSMO particles). All composites show higher coercivity and lower saturation magnetization as compared with standard CF samples. Composites having composition of 70 mol% LSMO: 30 mol% CF ball-milled samples show higher coercivity of 1080 Oe among all composites due to its different microstructure, where LSMO is acts as pinning center. This composite is showing better magnetic properties as compared to other composites and could be most applicable for practical application.

Keywords: Microwave-assisted synthesis; CMR-ferrite nanocomposites; Coercivity; Microstructure.

List of Figures

List of Tables

Chapter-1

General Introduction

Structure and properties of manganites

Structure and properties of ferrites

Importance of manganite-ferrite nanocomposite

1.1 Structure and properties of manganites

The manganites have attracted the attention of researchers from the technological as well as theoretical point of view. The perovskite manganites of the general formula $RE_{1-x}A_xMnO_3$ (RE = trivalent rare earth element such as La, Pr etc and A = divalent alkaline earth ions such as Ca, Sr, Ba etc.) has taken considerable interest in recent years as they exhibit simultaneous magnetic and electrical transitions in certain composition ranges. In perovskite structure, (RE, A) element occupy the A-site position (corner of a cube) and Mn occupies the B-site position (body center of a cube). All the face centered positions are occupied by oxygen [1-4].

Depending on the composition, manganite shows a variety of magnetic and electric phenomena, including ferromagnetic, antiferromagnetic, charge, and orbital ordering [5]. If the site *A* is partially occupied by one divalent atom such as Ca or Sr, then Mn^{3+} and Mn^{4+} coexist in the samples and the compounds show different behavior as the temperature is changed. The perovskite manganites have spurred considerable interest in recent years because of their colossal magnetoresistance (CMR) behavior [6]. Magnetoresistance (MR) in materials is of enormous technological importance, as these materials can be used as read heads for hard disks, magnetic storage and sensing devices [7]. The effectiveness of these materials is directly related to the percentage change of resistance in an external magnetic field. A negative MR was first found in perovskite manganites, exhibiting huge decrement in electrical resistivity in the presence of magnetic field. The most studied CMR systems are $La_{1-x}Sr_xMnO_3$ (LSMO) and $La_{1-x}Ca_xMnO_3$ (LCMO). The oxygen has a full outer shell (2p) being in O^{-2} state. Mn present in two oxidation states Mn^{+4} and Mn^{+3}, namely this is mixed valency compound $A_{1-x}^{3+}\, B_x^{2+}\, Mn_{1-x}^{3+}\, Mn_x^{4+}\, O_3^{2-}$. In order to get charge neutrality the ratio, Mn^{+3}/Mn^{+4} is equal to A^{+3}/B^{+2}. Therefore doping with atom B is equivalent to change the valency from +3 to +4.

At low temperature resistivity is metallic both in magnitude as well as in its dependence on temperature. With increase of temperature, it increases up to a temperature, T_{MI} (called metal-insulator transition temperature) beyond which it decreases having a negative temperature coefficient of resistance while maintaining a large magnitude. This metal to insulator transition at this temperature T_{MI} usually accompanied by ferromagnetic to paramagnetic transition.

A composition of x~0.33 is ideal to observe a good metal-insulator transition and negative colossal magnetoresistance (CMR) [8]. The coexistence of metallic conductivity and ferromagnetic coupling in these materials at low temperature has been explained in terms of a double exchange (DE) mechanism, proposed by Zener [9]. The basic process in this mechanism is the hopping of a d-hole from Mn^{4+} (d^3, t_{2g}^3, e_g^0, S=3/2) to Mn^{3+} (d^4, t_{2g}^3, e_g^1, S=2) via the oxygen, so that Mn^{+4} and Mn^{+3} ions change places.

$La_{0.67}Sr_{0.33}MnO_3$ (LSMO) is somewhat different from $La_{0.67}Ca_{0.33}MnO_3$ (LCMO). In LSMO case, the A-site ion size is being larger. The ferromagnetic metallic regime in LSMO extends over larger values of x. LSMO possesses the highest value of curie temperature (T_c = 370K) and combines low carrier density (10^{21} to10^{22} cm^{-3}) with a high spin polarization of charge carriers among CMR materials, which makes it very promising in room temperature application [10,11].

1.2 Structure and properties of ferrites

Ferrites, a ferrimagnetic ceramic compound having spinel type structure. Spinel ferrites are widely applied in areas due to a special combination of their physical properties and characteristics determined in numerous studies [12]. The magnetic properties of these ferrites arise largely from their structural features and the nature of the distribution of the ions in the sublattices. The spinel minerals have the generic formula AB_2O_4, where 'A' is a divalent ions such as Ni^{2+}, Co^{2+}, Mg^{2+}, Fe^{2+}, Mn^{2+}, Zn^{2+} and 'B' is a trivalent ions such as Fe^{3+} and Al^{3+}. The structure of spinels was described as having an oxygen ion sub lattice arranged in a cubic close-packed arrangement with cations occupying various combinations of the octahedral (O) and tetrahedral (T) sites. The cubic unit cell is large, comprising 8 formula units and containing 32 O and 64 T sites. Spinels are divided into two categories such as normal and inverse spinel. In normal spinel, the divalent cations 'A' are located on the tetrahedral (T) sites and the trivalent cations 'B' on the octahedral (O) sites. Generally Zn, Cd etc prefers normal spinels. $NiFe_2O_4$ (NF) or $CoFe_2O_4$ (CF) has an inverse spinel crystal structure. In the case of an inverse 'A' cation occupies one half of the octahedral coordination sites and half the 'B' cation occupies the other half 'O' sites as well as all 'T' sites. In spinels, the interaction between A and B atoms is always almost antiferromagnetic (they have opposite spins) so they cancel one another and the rest of

Fe^{+2} ions are aligned in the same direction with field so they are responsible for net magnetization [13].

In terms of magnetic properties, ferrites are often classified as "soft" and "hard" which refers to their low or high corecivity of their magnetism, respectively. Soft magnetic materials are used in devices (such as transformer core) that are subjected to alternating magnetic field and in which energy loses must be low. Soft magnetic materials have high initial permeability and low corecivity (easily magnetized and demagnetized). Low value of corecivity, gives easy movement of domain walls but they are restricted by the structural defects like voids or any nonmagnetic phases, so soft magnetic materials are must be free of such structural defects. They have also high electrical resistivity. Hard magnetic materials are utilized in permanent magnets, which must have a high resistance to demagnetization. It has high remanence, corecivity, saturation flux density as well as low initial permeability and high hysteresis energy loss [14, 15].

CF is a well-known hard magnetic material with high corecivity and moderate magnetization. These properties along with their great physical and chemical stability make CF suitable for magnetic recording applications such as audio and video tapes and high density digital recording disks [16, 17].

1.3 Importance of manganite: ferrite nanocomposites

Nanocomposites of manganite, a colossal magnetoresistance perovskite and ferrite an insulating magnetic oxide are of interest because of their unusal magnetic as well as electrical properties [18, 19]. Nanocrystalline materials are single phase or multiphase polycrystals, where the crystal size is of the order of few nanometers so that about 40 to 80 % of the atoms are in the grain boundaries and the properties are dramatically different from their bulk scale counterparts [20]. Important among these nanoscale materials are nanocomposites, in which the constituents are mixed at nanometer scale. The study of nanocomposite materials requires a multidisciplinary approach with impressive technological promise, involving novel synthesis techniques and an understanding of physics and surface science [21, 22].

Nanocomposites of manganite: ferrite samples consist of CMR manganite phase and an insulating oxide secondary phase. The reason for studying such composites is that the presence of the insulating phase forces the electric current to meander through the CMR grains, thereby increasing significantly the contribution of the grain boundaries to the conduction process [23]. This leads, in turn, to an enhancement of electrical and magnetic properties. Due to both fundamental and significant technological importance, the research on manganite-ferrite nanocomposites has been very actively developed in recent years [24].

Chapter -2
Literature Survey

Synthesis of manganite: ferrite composite by various routes
Importance of microwave-assisted synthesis route
Microwave-assisted synthesis of manganite: ferrite nanocomposite
Summary of literature review
Objective of present studies

2.1 Synthesis of manganite: ferrite nanocomposites by various routes

Many works have been devoted to understand the structural and physical properties of the manganite-ferrite based nanocomposite materials. The remarkable electrical and magnetic properties of these composites are of considerable interest for a new generation of magnetic sensors and recording devices. The different methods used for enhancing these electrical and magnetic properties are: substitution doping [25], grain size reduction [26, 27], distribution of the manganite grains in a non-magnetic insulating matrix and magnetic insulating matrix [28].

Zie et al. have studied on LSMO: $SrFe_{12}O_9$ nanocomposite system [29] by chemical co-precipitation method. The composites of LSMO: SFO were prepared using solid-state sintering. In this work, it is possible to enhance spin disorders at the grain boundaries and interfaces of LSMO grains by introducing a second magnetic material into LSMO grains in order to enhance electrical and magnetic properties.

Xiong et al. [30] have studied $La_{0.7}Ca_{0.2}Sr_{0.1}MnO_3$ (LCSMO)/$CoFe_2O_4$ (CFO) composites, which were prepared by a standard ceramic technique. Compared with pure LCSMO, the MR effect of the composites is enhanced in low magnetic fields of 3 kOe at a wide temperature range below T_c. The enhanced MR at low field (LFMR) is related to the enhancement of spin-dependent tunneling of electrons and spin-dependent scattering at the surfaces between LCSMO grains.

Yan *et al.* [31] have investigated the LFMR of the LSMO/CF composite for a single composition of 20 wt% CF. The resistivity of the composite is about an order of magnitude larger than that of the same grain-sized pure LSMO. A large LFMR has been obtained in this composite compared to pure LSMO. Since the spin-dependent scattering of the conduction electrons at the grain boundaries is highly field sensitive, the magnetic scattering of the polarized charge carriers may be responsible for the electrical and magnetic properties.

Another interesting system with a hard ferromagnetic insulator (HFMI) as the second phase of the composite is reported by Huang *et al.* [32] They have studied $(L_{0.67}Sr_{0.33}MnO_3)_{1-x}$ / $(BaFe_{11.3}(ZnSn)_{0.7}O_{19})x$ (BAM) composites as a function of vol.% (0.0–1.0) of the insulating phase. In this work, it was suggest that magnetic coupling is not solely responsible for increase in MR at low field, but microstructure also plays an important role to have the desired effect.

2.2. Importance of microwave-assisted synthesis route

Microwaves are electromagnetic waves with wavelengths from 1 mm to 1 m and corresponding frequencies between 300 MHz and 300 GHz. 0·915 GHz and 2·45 GHz frequencies are commonly used for microwave heating [33, 34]. These frequencies are chosen for the microwave heating based on two reasons. The first is that they are in one of the industrial, scientific and medical (ISM) radio bands set aside for non-communication purposes. The second is that the penetration depth of the microwaves is greater for these low frequencies [35]. Generally, materials can be classified into three categories based on their interaction with microwaves: (1) materials that reflect microwaves, typified by bulk metals and alloys, e.g. copper; (2) materials that are transparent to microwaves, typified by fused quartz, several glasses, ceramics, Teflon, etc.; and (3) materials that absorb microwaves which constitute the most important class of materials for microwave synthesis, e.g. aqueous solution, polar solvent, etc. [36].

In microwave heating, unlike conventional heating, heat is generated internally within the material instead of originating from external sources. As a result of internal and volumetric heating, thermal gradients and direction of heat flow in microwave heated materials can be just the opposite of those in conventional methods**.** It offers a clean, cheap and convenient method of heating often resulting in higher yields and shorter reaction times.

Applications of microwave processing are indeed very wide. For instance, it can include processing of solution and suspension, drying, organic material burnout, clinkering, sintering of ceramics and ceramic composites, preparation of specialty ceramics, plasma processing, processing of polymers and polymer composites, fabrication of functionally graded materials, joining, fiber drawing, melting, reaction synthesis of ceramics and a host of very promising, new, advanced applications [37]. The advantages of this technology have, more recently, also been exploited in the context of multistep total synthesis and medicinal chemistry/drug discovery , and have additionally penetrated related fields such as polymer synthesis, material sciences, nanotechnology and biochemical processes. The use of microwave irradiation in chemistry has thus become such a popular technique in the scientific community that it might be assumed that, in a few years, most chemists will probably use microwave energy to heat chemical reactions on a laboratory scale. The statement that, in principle, any chemical reaction that requires heat can

be performed under microwave conditions has today been generally accepted as a fact by the scientific community.

David et al. [38] investigates about the microwave synthesis which has been modified so that syntheses involving the refluxing of organic solvents can be safely and conveniently under taken. For solution reactions the most promising results have been obtained by using sealed Teflon containers, which can sustain temperature up to 250^0C and pressure up to 80 atm. The reaction time for the modified reflux system are longer than those obtained in the Teflon containers, in which the temperature is sometimes more than 100^0C higher than the reflux temperature because of the high pressure induced, but they are frequently shorter than those obtained with conventional heating techniques. In the past, microwave chemistry was often used only when all other options to perform a particular reaction had failed, or when exceedingly long reaction times or high temperatures were required to complete a reaction. This practice is now slowly changing and, due to the growing availability of microwave reactors in many laboratories, routine synthetic transformations are now also being carried out by microwave heating [39]. The areas where this technology has been applied include: process control, drying of ceramic sanitary wares, calcinations and decomposition of gaseous species by microwave plasma, powder synthesis, and sintering. Microwave processing of materials was mostly limited until 2000 to ceramics, semiconductors, inorganic and polymeric materials. There was a misconception between researchers that all metals reflect microwave or cause plasma formation, and hence cannot be heated, except exhibiting surface heating due to limited penetration of the microwave radiation. The researchers did not notice that this relation is valid only for sintered or bulk metals at room temperature, and not for powdered metals and/or at higher temperatures. Now it has been found that the microwave sintering can also be applied as efficiently and effectively to powdered metals as to many ceramics. This paper compares advantages of microwave sintering against conventional sintering and presents some applications confirming its advantages.

Microwave processing has gained worldwide acceptance as a novel method for heating and sintering a variety of materials, as it offers many advantages in terms of enhanced diffusion processes, reduced energy consumption and processing cost, very rapid heating rates and significantly reduced processing times, decreased sintering temperatures, improved physical and

mechanical properties, simplicity, unique properties, new materials and products and lower environmental hazards, which are not observed in conventional processes.

2.3. Microwave-assisted synthesis of manganite: ferrite nanocomposites

There are different syntheses techniques are used to prepare nanocomposite materials. Among all the synthesis techniques, microwave synthesis technique is now well documented. This technique is highly versatile and can be used for the synthesis of a wide variety of materials. Nayak et al. [40] have studied the properties of nanograined LCMO: NF ($NiFe_2O_4$) composites which are prepared in situ microwave refluxing technique. This technique has the inherent advantage of uniformly distributing the two phases and the two phases will also have a similar grain size distribution as they will be subjected to identical processing conditions. This will overcome the limitations of asymmetric grain sizes for the two phases encountered and thus facilitate study of possible electronic interactions between the two phases, LCMO and NF. The interesting aspect of these nanocomposites is that above the transition temperatures corresponding to LCMO phase, the nanocomposite will be electrically insulating but magnetic due to the presence of NF. Below the transition temperatures of LCMO the composite will be conducting and also magnetic with a CMR behavior. This temperature dependent behavior makes it attractive for innovative applications in magnetic information storage. The LCMO phase however loses its negative magnetoresistance behavior due to a substitution of Mn with either or both Ni and Fe. The electrical transition is suppressed for $x > 0.02$M NF while the magnetic transition is observed till $x = 0.15$M NF. The nanograin size of the LCMO phase has a significantly high grain boundary scattering, which leads to enhanced electrical and magnetic properties.

2.4. Summary of literature review

From literature it was found that:

- Doping in A or B site, creation of high density of disordered areas such as grain boundaries and distribution of the perovskite manganite in different matrices have been used as attractive approaches to enhance the electrical and magnetic properties of manganite-ferrite nanocomposites.

- Microwave refluxing is a novel technique to synthesize manganite-ferrite composites at a nano level scale for different applications.
- There are few literatures on the effect of ferrite addition on the electrical and magnetic properties of manganite by different synthesis routes.
- There are no literatures on the enhancement of magnetic properties (especially enhancement of coercivity) of manganite-ferrite nanocomposites, synthesized using microwave refluxing technique.
- There are no literatures on comparative study of microstructural and magnetic properties of in-situ and ball milled synthesized LSMO: cobalt ferrite nanocomposites using microwave oven.

2.5. Objective of present studies

The main objectives of present studies are:

- Study the effect of $CoFe_2O_4$ (CF) addition on microstructural and magnetic properties of $La_{0.67}Sr_{0.33}MnO_3$ (LSMO): CF nanocomposites by microwave-assisted synthesis route.
- Comparative study of microstructural and magnetic properties of in-situ and ball milled synthesized LSMO: CF nanocomposites by above said synthesis routes.

Different compositions of (1-x) mol% LSMO: x mol% CF composites (where x= 0, 30, 50 70 and 100) have been synthesized using kitchen microwave oven through in-situ and ball milled process. Different characterizations such as DSC-TG, XRD, SEM with EDAX, particle size analyzer and MH loop have been performed and the results are discussed in detail.

Chapter – 3

Experimental

Microwave-assisted in-situ synthesis of LSMO and CF as well as
LSMO: CF nanocomposites
Microwave-assisted synthesis of ball milled LSMO: CF nanocomposite
General characterization
Thermal, x-ray diffraction (XRD), scanning electron microscope (SEM), density, magnetization, particle size measurement

3.1. Microwave-assisted in-situ synthesis of LSMO and CF as well as LSMO: CF composites

For preparation of pure LSMO powder, stoichiometric equivalents of La-acetate, Sr- chloride and Mn-acetate were mixed with ethylene glycol and this mixture is used as a precursor I. For preparation of pure CF powder, stoichiometric equivalents of cobalt chloride and Iron chloride were mixed with ethylene glycol and this mixture is used as a precursor II. For the composite case (composition mention in objective section of chapter 2) i. e. precursor III is the mixture of precursor I and II.

The individual precursor solution was kept at 80 °C under constant stirring condition. These solutions were found to be slightly acidic and also turbid. The pH of this acidic precursor solution was increased by addition of KOH solution. The initially turbid solution becomes clear and form a gel at pH = 11. These gel precursors were taken for further processing by microwave refluxing. A commercial microwave generator operating at 2.5 GHz and 980 Watts was used to heat the precursor solution to > 473 K, boiling point of ethylene glycol. This was later condensed by refluxing with circulating water and recycled. The solution was subjected to microwave heating and refluxing for a period of 1hour and the precipitate obtained was washed thoroughly washed with distilled water and dried. The dried powders were calcined at 800°C for 1hour. The calcined powder was pelletized and annealing was done at 1200 °C for 2h. Structural, microstructural and magnetic properties of these annealed samples have been studied in detail in chapter 4 section 4.2.

3.2 Microwave-assisted synthesis of ball milled LSMO: CF composites

Microwave-assisted synthesized pure LSMO and CF calcined powders were mixed in appropriate proportion as mentioned in objective section of chapter 2. The different composite powders are ball milled separately in a high energy planetary ball mill at a speed of 350 rpm. Milling was carried out for 2 hours in wet condition (about 50 ml of ethanol) to prevent undue oxidation. These powders were pelletized and annealing was done at 1200 °C for 2h. Structural, microstructural and magnetic properties of these annealed samples have been studied in detail in chapter 4 section 4.3.

3.3 GENERAL CHARACTERIZATION

3.3.1. Thermal

Thermal analysis were carried out using thermogravimetric and differential scanning calorimetric (TG-DSC) by heating the sample at 10 °C/min in argon in a thermal analyzer (Model STA 4096, NETZSCH , Germany).

3.3.2. X-ray diffraction

Phase analysis was studied using room temperature powder X-ray diffraction (Model: PW 1830 Diffractometer, Phillips, Netherland) with filtered 0.154056 nm Cu Kα radiation. Samples are scanned in a continuous mode from 20° – 80° with a scanning rate of 0.04 (°) / 1 (s).

3.3.3. Scanning Electron Microscope

Microstructural features along with chemical compositions (using EDAX) were studied using Scanning Electron Microscope (JSM 6480 LV JEOL, Japan). For preparation of SEM sample, the pellets placed in acetone in an ultra sonication bath (20 kHz, 500 W) for half an hour. These pellets after sonication were used for microscopy. The images were taken in back scattered electron (BSE) mode to distinguish the two phases present in the composites.

3.3.4. Density

Density was measured by using vacuum assisted soaking of pellets in kerosene medium for about 2hr. The dry weight, suspended weight, and soaked weight were taken to calculate bulk density using the following formula.

$$\text{Bulk Density} = \frac{D}{W-S} \times \text{density of liquid medium}$$

Liquid medium in our case is kerosene with density of 0.80 g/cm^3. Where, D, W, S stands for dry weight, soaked weight and suspended weight respectively of the sample.

3.3.5. Magnetization

Pulse field hysteresis loop tracer (MAGNETA) was used to trace MH loop for sintered pellets. MH loop can measure up to a magnetic field of 0.5 Tesla. The machine was first calibrated using standard sample having saturation magnetization of 72.4 emu/g.

3.3.6. Particle size measurement

Particle size of the samples is usually obtained with the help of scanning electron microscopy (SEM). The particle size of sample is also determined using particle size analyzer (Malvern, UK).

The crystallite size corresponds to the mean value of the crystalline domain size of the particles is determined from the X-ray line broadening using Debye-Scherrer formula with correction factor as given below,

$$D_x = \frac{0.9\,\lambda}{\beta\,cos\theta}$$

Where D_X is average crystalline size, λ is the X-ray wavelength used, β the angular line width of half maximum intensity and θ the Bragg's angle in degree.

Chapter – 4

Results & Discussion

Microstructural and magnetic properties of microwave-assisted synthesized LSMO and CF nanopowders

Characterization (DSC-TG, XRD, SEM, Particle size analysis, Density, Magnetization)

Microwave-assisted synthesized LSMO: CF nanocomposite

Characterization (XRD, SEM, Particle size analysis, Density, Magnetization)

Microwave-assisted synthesis of ball milled LSMO: CF nanocomposite

Characterization (XRD, SEM, Particle size analysis, Density, Magnetization)

4.1 Microstructural and magnetic properties of microwave-assisted synthesized LSMO and CF nanopowders

In this section, pure phase of LSMO and CF have been synthesized by microwave refluxing process. The detail experimental procedure was described in Chapter 3, section 3.1**.** Calcination temperature determination, phase purity, particle morphology, particle size distribution, density and magnetization have been studied using DSC-TG, XRD, SEM, particle size analyzer, Archimedes principle and M-H loop, respectively. In this section, thermal, structural, microstructural and magnetic properties of pure phase LSMO and CF nanopowders were discussed in detail.

4.1.1 Thermal

Fig. 4.1 (a) and (b) show the DSC-TG curves of as-synthesized LSMO and CF powders, respectively. Three distinct regions (30°C-250°C; 300°C-400°C and 400°C-600°C) of major weight loss were observed for both LSMO and CF powders as seen from TG curves of Fig. 4.1. The total weight loss starting from room temperature to 900°C for both powders is found to be around 17% (for LSMO) and 19% (for CF). This weight loss is due to the removal of physically absorbed or chemically adsorbed water or removal of some organic compounds present in the samples, confirmed from the endothermic peaks (100°C, 300°C-360°C, 400°C-600°C) in DSC curves of both powders. The minor weight loss as well as broad exothermic peak starting from 700°C to 800°C for both samples confirms the crystallization temperature of these powders. So, from the thermal results, it was confirmed that the optimum temperature of calcination to get a phase pure LSMO and CF nanopowders is around 800°C.

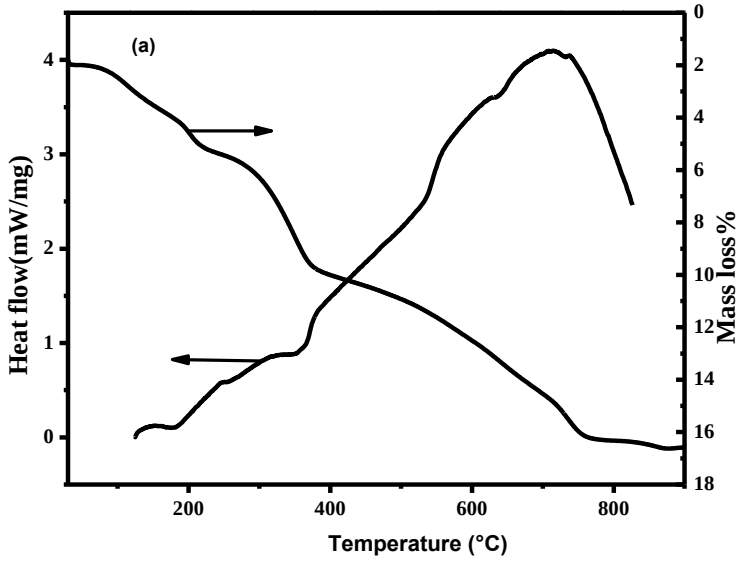

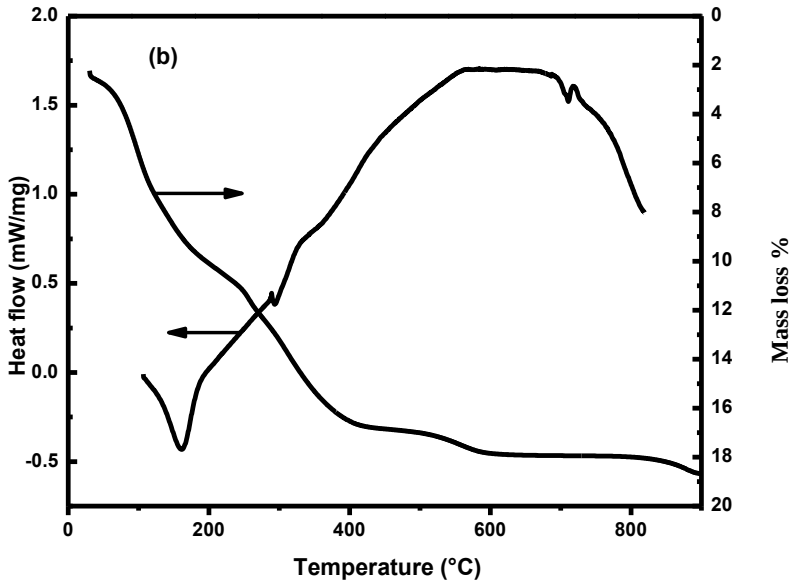

Fig. 4.1: DSC-TG curves of as prepared (a) LSMO and (b) CF powders

4.1.2 Structural

Phase purity of LSMO and CF powders was confirmed from the X-ray diffraction patterns. The as-synthesized powders of LSMO and CF are amorphous in nature. These amorphous powders were calcined at 800°C and found to be crystalline in nature. To study the microstructure, density as well as magnetic properties of these samples, the calcined powders were pelletized and sintered at 1200 °C for 2h. Fig. 4.2 (a) and (b) show the XRD patterns of sintered LSMO and CF pellets, respectively. All the peaks are identified with the help of JCPDS and index with monoclinic phase of LSMO (JCPDS file no: 72-0841) and cubic phase of CF phase (JCPDS file no: 22-1086). The crystallite size of LSMO and CF is found to be around 34 and 50 nm, respectively using Scherrer's formula. The lattice parameters and cell volume of LSMO and CF are given in Table 4.1.

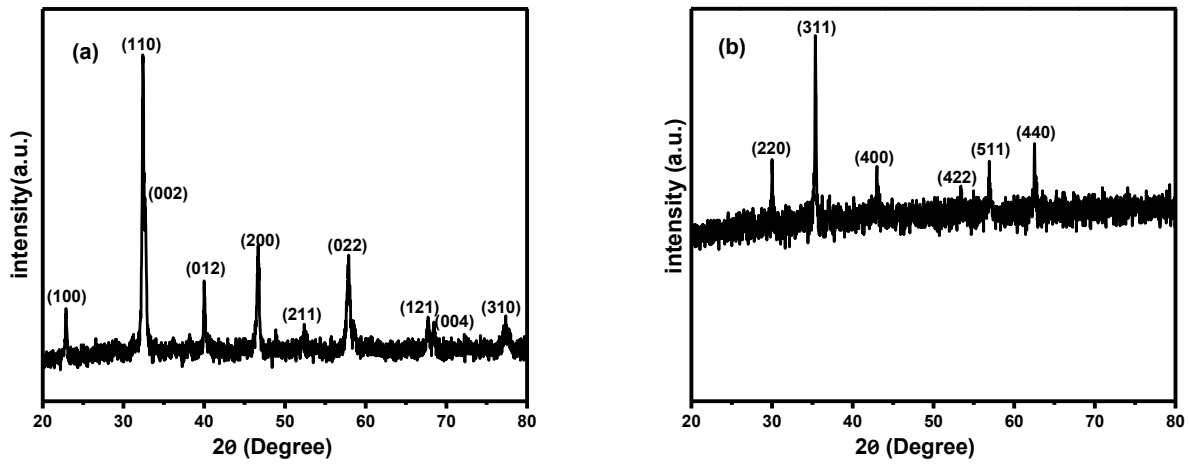

Fig. 4.2: X-ray diffraction patterns of sintered (a) LSMO and (b) CF pellets

Table 4.1 Phase, lattice parameters and cell volume of sintered LSMO and CF samples.

Samples	Phase	Lattice parameter (Å)	Cell volume (A^3)
LSMO	Monoclinic (m)	a=3.95Å, b= 3.99Å, c= 5.57Å and β = 101.24°	87.785
CF	Cubic (c)	a=b=c= 8.39 Å	590.58

4.1.3 Microstructural and particle size distribution

SEM micrographs in back scattered mode of sintered LSMO and CF samples are shown in Fig. 4.3 (a) and (b), respectively.

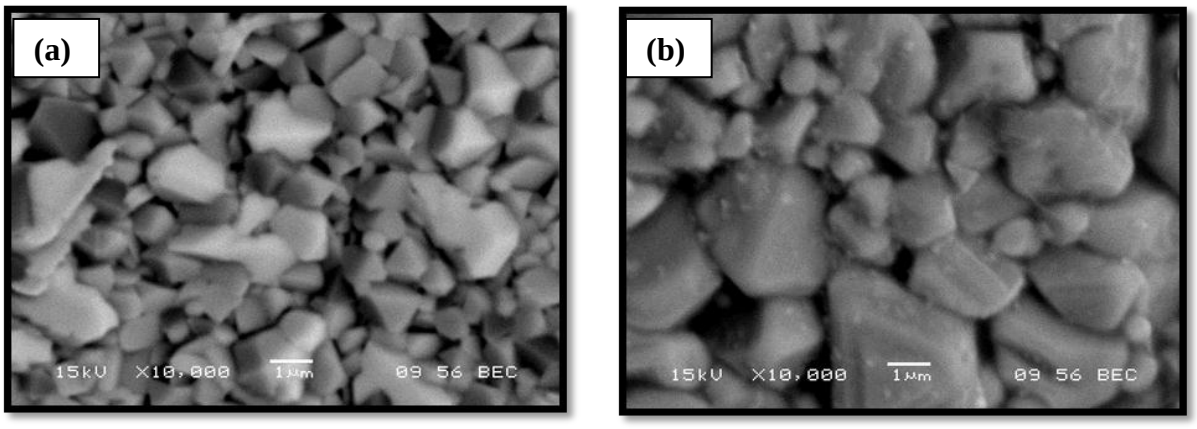

Fig. 4.3: SEM micrographs of sintered (a) LSMO (b) CF pellet.

The particle size of CF is comparatively large as compared to LSMO, as seen from the SEM micrographs. The particle of LSMO samples show a mixture of triangular, square, diamond, irregular flakes and spherical (few numbers) in shape. However, the particle of CF is nearly spherical with multi-facet in nature. The particle size distribution of LSMO and CF calcined (1200°C) powders using particle size analyzer is shown in Fig. 4.4 (a) and (b), respectively. The average particle size of LSMO (in the range 200-300 nm) is comparatively lower than CF (in the range 400-500 nm). Narrow particle size distribution for LSMO and wide for CF as observed from the particle size distribution graphs.

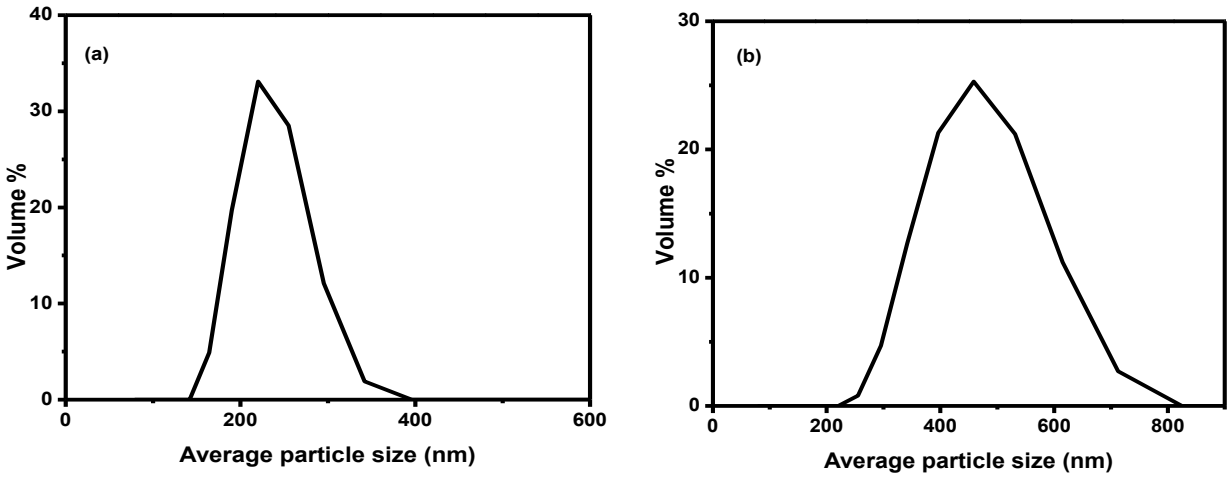

Fig. 4.4: Particle size distribution of (a) LSMO and (b) CF

Density of LSMO and CF was calculated using Archimedes principle and is given in Table 4.2. The density is strongly related to the microstructure and it was found that LSMO is comparatively more density than CF due to small particle size as well as distribution and shape.

.

Table 4.2: Density of CF and LSMO

Phases	Dry weight (g)	Suspended weight (g)	Soaked weight (g)	Density (%)
Pure CF	0.5630	0.4807	0.5817	84
Pure LSMO	0.5814	0.5040	0.5841	87

4.1.4 Magnetization

Magnetization as a function of field (M-H loop) for CF pellets is shown in Fig. 4.5. M-H loop of LSMO is not able to measure due to its paramagnetic nature at room temperature. The coercivity (H_c) and saturation magnetization (M_s) of pure CF were found to be ~ 291 Oe and 75.9 emu/g, respectively.

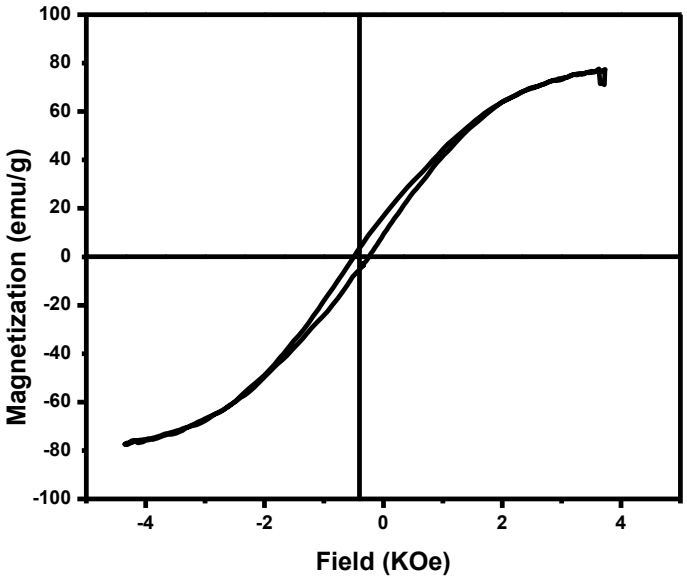

Fig. 4.5: Room temperature M-H loop of pure CF

4.1.5 Summary

LSMO and CF powders were successfully prepared by using microwave refluxing. DSC- TG result confirms that 800°C is the optimum temperature for calcination to obtain a pure phase LSMO and CF. In structural study, all the peaks are identified with either LSMO or CF without any impurity or secondary phases and also indicating that LSMO phase corresponds to monoclinic phase whereas CF is cubic. The particle shape of pure LSMO shows mixture of irregular shape with different morphology where as pure CF shows irregular morphology with a larger size. In magnetization study, the H_c and M_s of CF were found to be ~ 291 Oe and 75.9emu/g, respectively at room temperature, which matches with the standard CF samples.

4.2 Microstructural and magnetic properties of microwave-assisted synthesized LSMO: CF nanocomposites

This section describes the synthesis of (1-x) mole % LSMO: x mole % CF (where x = 30, 50 and 70) composite by using microwave refluxing technique. The detailed experimental procedure is explained in chapter 3, section 3.1. Structural, microstructural, particle size distribution, density and magnetic properties are described in detail.

4.2.1 Structural

XRD patterns of sintered LSMO: CF composites with different molar percentage are shown in Fig. 4.6.

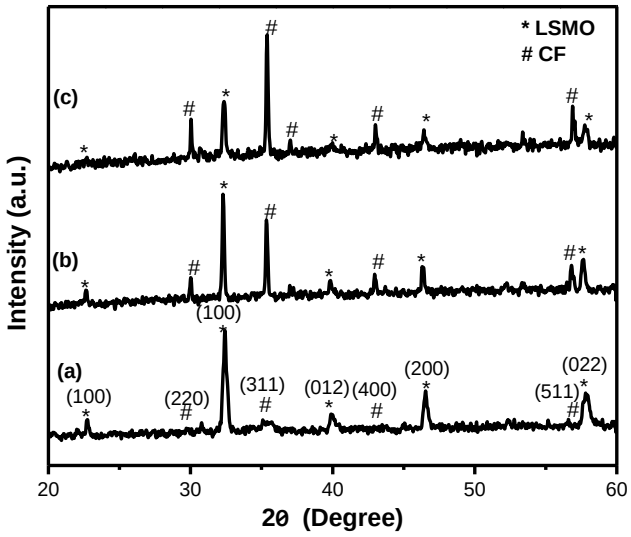

Fig. 4.6: XRD patterns of (a) 70LSMO: 30CF, (b) 50LSMO: 50CF and (c) 30LSMO: 70CF composite pellets

All the peaks are identified with either LSMO (orthorhombic) or CF (cubic) as mentioned in the XRD patterns with the help of JCPDS (file no: 72-0841 for LSMO and 22-1086 for CF). No secondary phase has been detected, indicating that interfacial reactions between LSMO and CF grains are negligible. With increasing CF percentage, the intensity of (100) plane (2θ = 32.23) reflection from the LSMO phase decreases, where as the intensity of (311) reflection from the CF phase gradually increases. To observe the peak shift of LSMO (2θ = 32.23), slow scan of these composites are performed and XRD patterns are shown in Fig. 4.7.

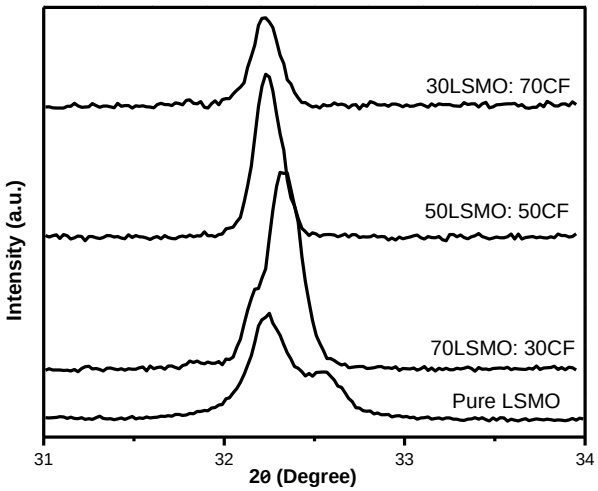

Fig. 4.7 Slow scan XRD patterns of LSMO and LSMO: CF composites

There was a structural transition from monoclinic to orthorhombic form of LSMO as seen from the slow scan XRD patterns. Shifting of (100) plane of LSMO towards lower angle with increasing CF content indicates the change in lattice parameter and cell volume (see Table 4.3).

Table 4.3: Lattice parameter and cell volume of sintered LSMO: CF

(1-x)LSMO: x CF composite	Phase	Lattice parameter (Å)	Cell volume
70LSMO:30CF	LSMO(O) CF (C)	a= 7.08 b= 8.69 c= 8.98 a=b=c= 8.39	552.5
50LSMO:50CF	LSMO(O) CF(C)	a= 6.42 b= 7.84 c= 8.58 a=b=c= 8.39	431.8
30LSMO:70CF	LSMO(O) CF (C)	a=5.06 b= 7.34 c= 8.39 a=b=c= 8.39	311.6

Note: O represents orthorhombic structure of LSMO and C represents cubic structure of CF

4.2.2 Microstructural and particle size distribution

Phase distribution and morphology were performed using back-scattered mode SEM on the sintered LSMO: CF composites. Fig. 4.8 (a), (b) and (c) shows the SEM micrographs along with EDAX as well as number of grains as a function of grain size (from SEM micrographs) for the composites 70 mol% LSMO: 30 mol% CF, 50 mol% LSMO: 50 mol% CF and 30 mol% LSMO: 70 mol% CF, respectively.

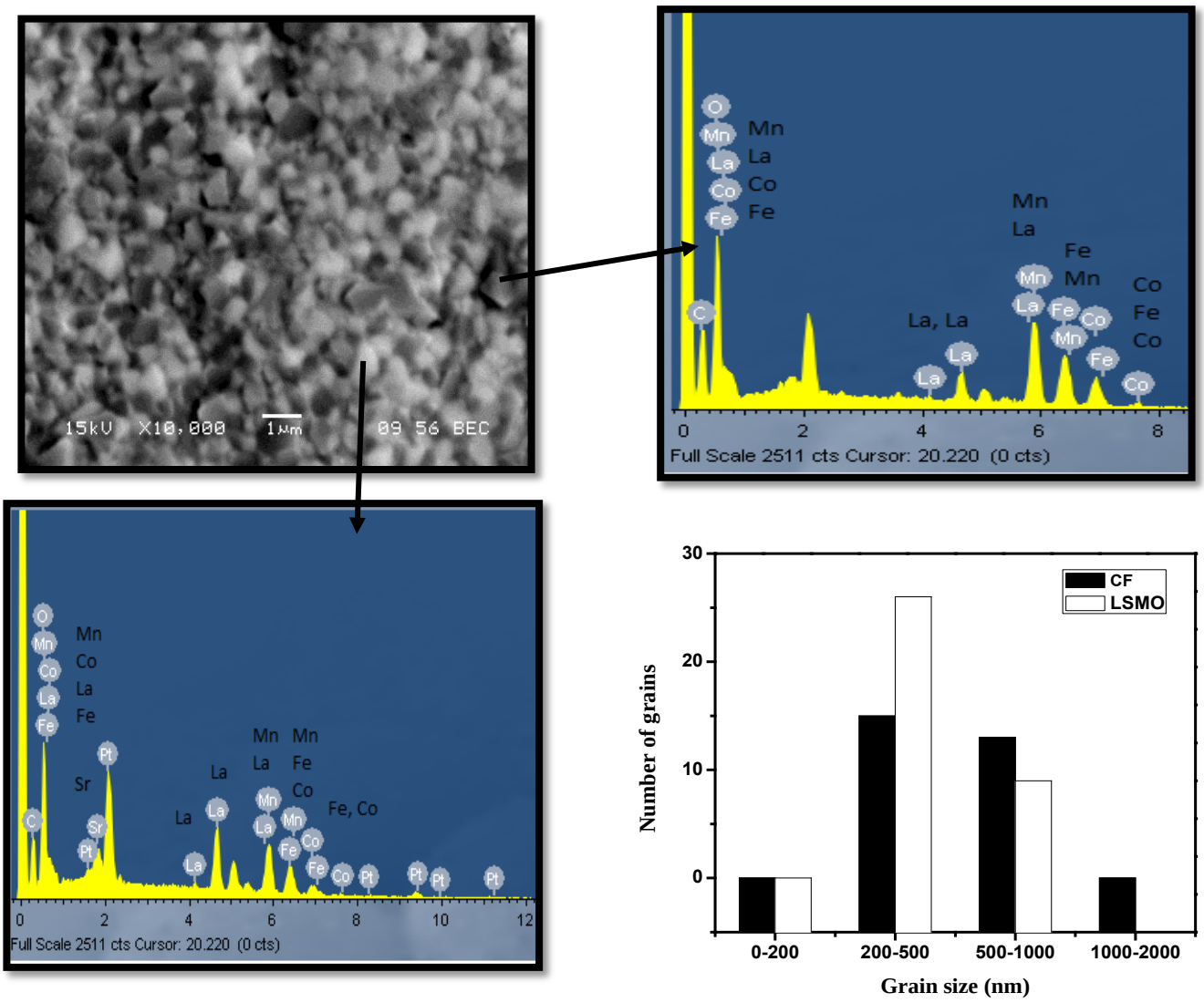

Fig.4.8 (a): SEM micrograph, EDAX and number of grains as a function of grain size for 70 mol% LSMO: 30 mol% CF composites

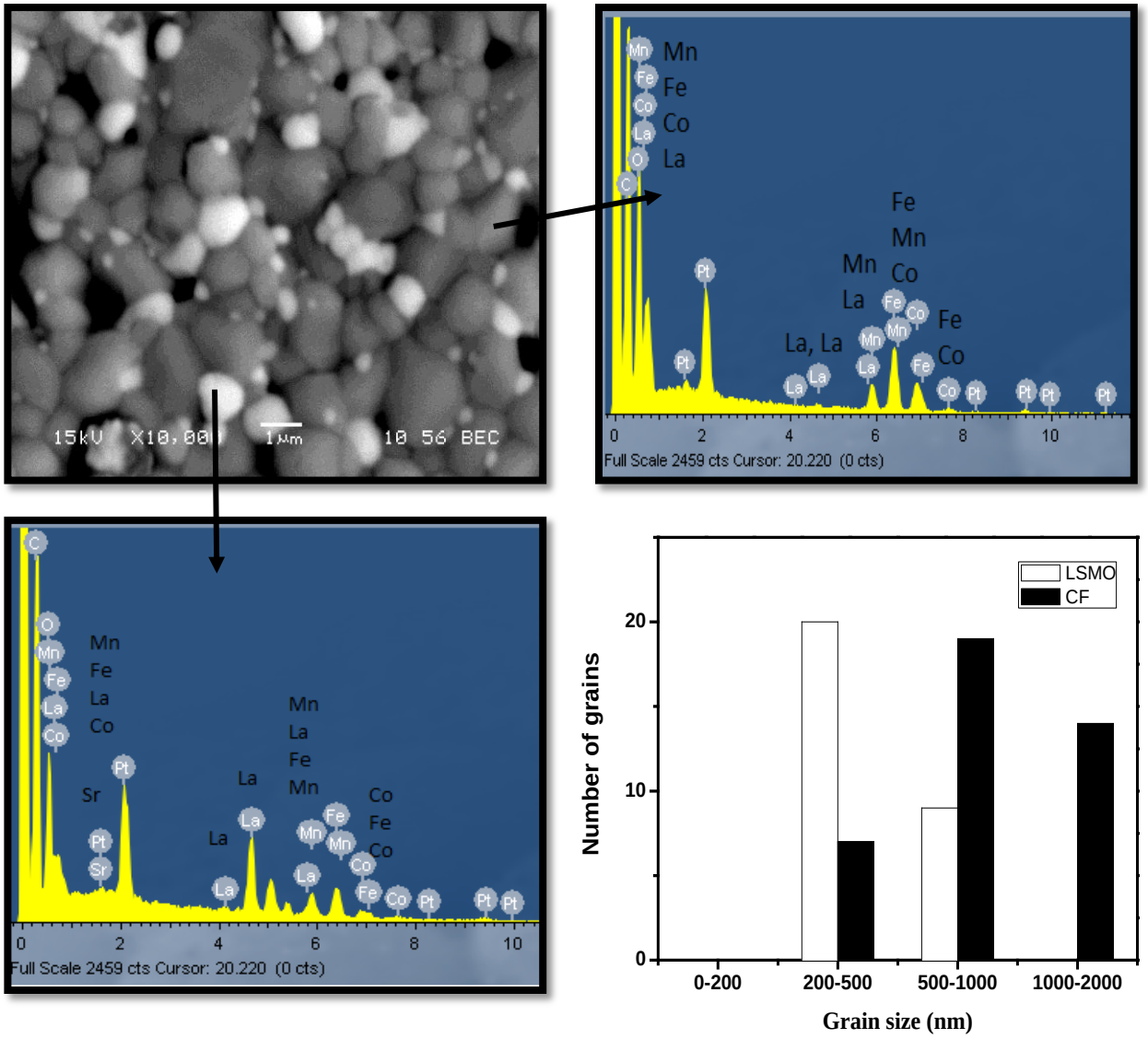

Fig. 4.8 (b): SEM micrograph, EDAX and number of grains as a function of grain size for 50 mol% LSMO: 50 mol% CF composites

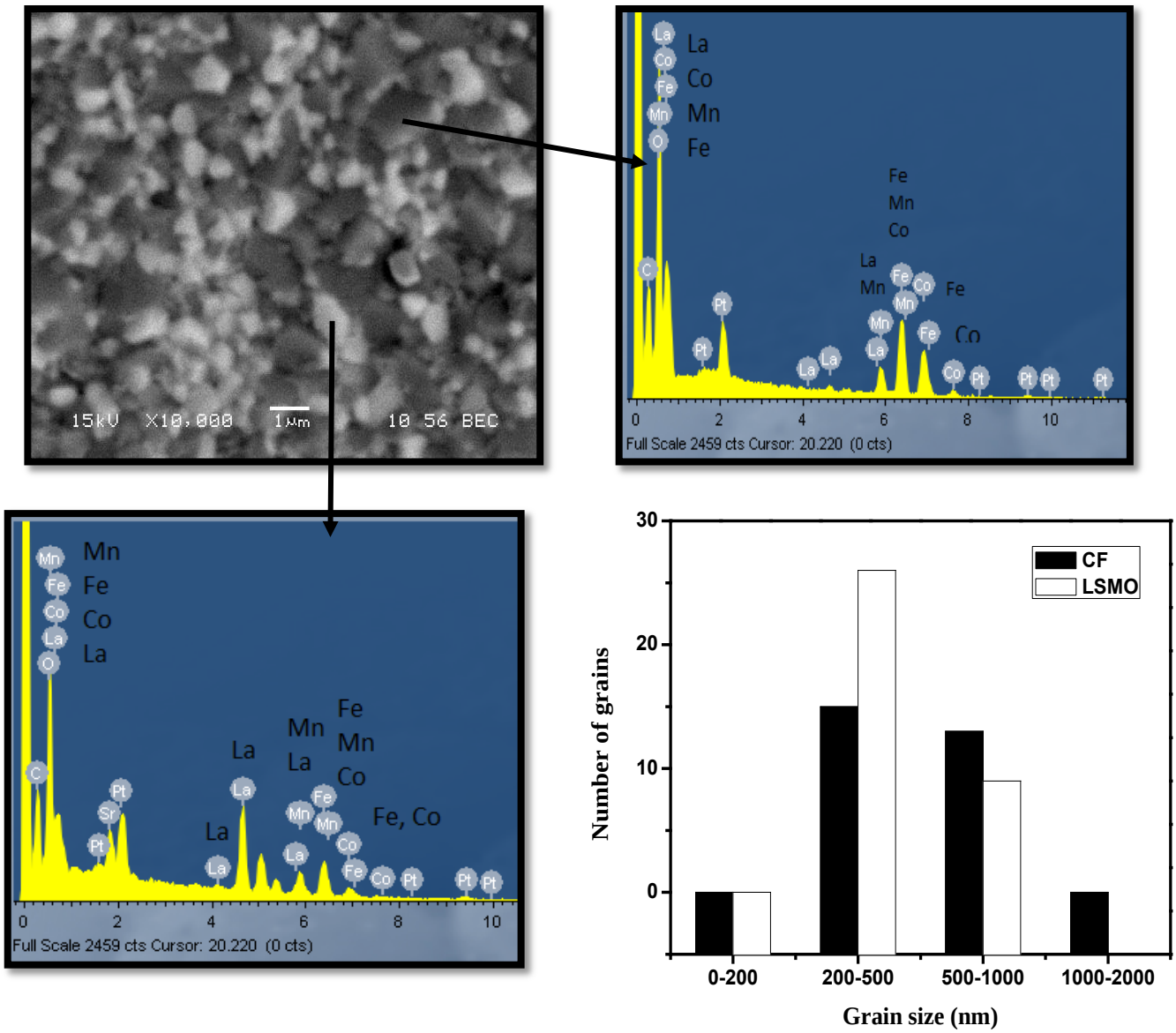

Fig. 4.8 (c): SEM micrograph, EDAX and number of grains as a function of grain size for 30 mol% LSMO: 70 mol% CF composites

The LSMO: 30 mol % CF and 70 mol % CF have similar microstructure (irregular multi-facet shape), whereas LSMO: 50 mol% CF composites have different morphology (nearly spherical) as seen from the SEM micrographs. From back-scattered images as well as EDAX analysis, it was confirmed that the white portions indicates the presence of LSMO and the black portion indicates the presence of CF. From microstructural analysis, it was also confirmed that the number of grains are in the range between 200 nm to 500 nm for all composites. Maximum number of grains is in the range of 200 nm for LSMO and for CF, the range is above 500 nm.

Particle size distribution for all composites are done using particle size analyzer and the average particle size of these composite are found to be in the range between 200 nm to 300 nm. Typical volume percentage as a function of average particle size (nm) for 30 mol % LSMO: 70 mol% CF is shown in Fig. 4.9.

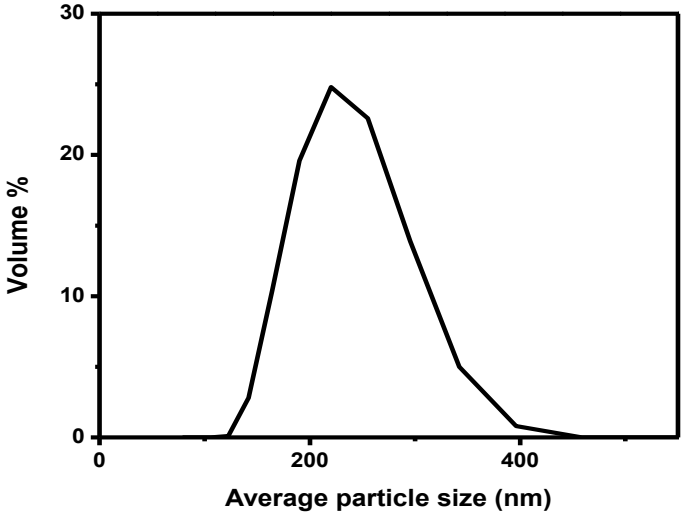

Fig. 4.9: Particle size distribution of 30 mol% LSMO: 70 mol% CF composite

The density of all sintered composites is given in Table 4.5. More than 90% density was observed for all composites due to its morphology. Density increases with increase in CF content and highest density was obtained for 70 mol % CF addition.

Table 4.5: density of pellets 70LSMO:30CF, 30LSMO:70CF and 50LSMO:50CF

LSMO: CF (mol %)	Dry weight (g)	Suspended weight (g)	Soaked weight (g)	Density (%)
70:30	0.5986	0.5159	0.6	91.7
50:50	0.4961	0.4229	0.4971	94.3
30:70	0.4858	0.4149	0.4863	95.7

4.2.3 Magnetization

The magnetization as a function of field at a room temperature for different composites (30 mol%, 50 mol% and 70 mol% CF content) are shown in Fig. 4.10.

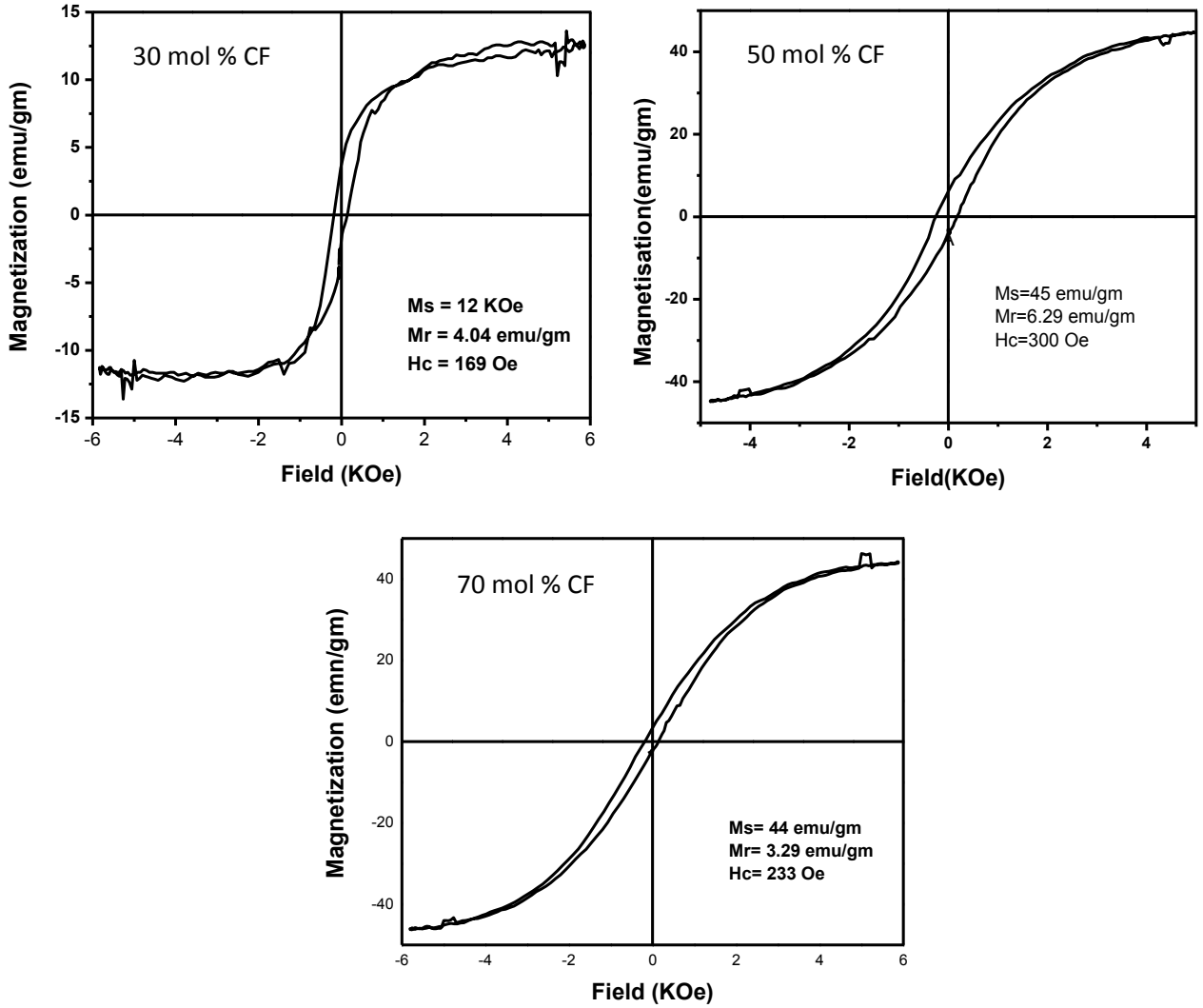

Fig. 4.10: Room temperature M-H loop of LSMO: CF composites

Table 4.6 summarizes the magnetic data of the LSMO: CF composite. Certain microstructure of composite plays a very important role in the enhancement of magnetic properties [41]. The saturation magnetization increases due to the increase of ferromagnetic order of CF [42], since coercivity is strongly depends on the microstructural property such as defects, strains and non-magnetic phases in the material [43]. The 50 mol% LSMO: 50 mol% CF composite shows higher coercivity as well as higher saturation magnetization. This may be due to grain boundary pinning effect. Spin polarized intergrain pinning is due to magnetic disorder and magnetic coupling between LSMO and CF [44].

Table 4.4: Magnetic data of 30, 50 and 70 LSMO: CF composites sintered at 1200^0C

Samples	Coercivity Hc, (Oe)	Remanent magnetization M_r, (emu/gm)	Saturation magnetization M_s, (emu/gm)
70LSMO:30CF	169	4.04	12
50LSMO:50CF	300	6.29	45
30LSMO:70CF	233	3.29	44

4.2.4 Summary

Nanograined composite of LSMO and CF were successfully prepared using microwave refluxing synthesis technique. In composite LSMO shows orthorhombic crystal structure where as CF phase is cubic. Structural transition from monoclinic to orthorhombic LSMO was observed with the addition of CF content. The particle shape of 30 and 70 CF composites show irregular shape flake-like morphology, whereas 50 LSMO: 50 CF shows nearly spherical with flake-like morphology. The average particle size distribution of all composite are found to be in the range between 200 nm to 300 nm. The 50 LSMO: 50 CF composites show higher saturation magnetization as well as higher corecivity.

4.3 Microstructural and magnetic properties of ball milled LSMO: CF nanocomposites

In comparison point of view, the as-prepared pure LSMO and CF powders synthesized by microwave refluxing process were calcined at 800°C and mixed with the above compositions and ball milled for 2h. The structural, microstructural and magnetic properties of these ball milled composites are discussed in this section.

4.3.1 Structural

Fig. 4.11 shows the X-ray diffraction patterns of ball milled sintered LSMO: CF composite pellets with different molar percentages.

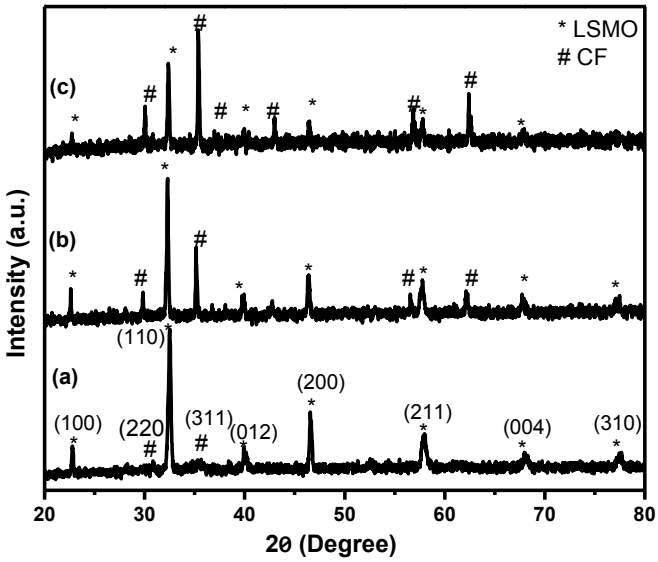

Fig. 4.11 XRD patterns of (a) 70LSMO: 30CF, (b) 50LSMO: 50CF and (c) 30LSMO: 70CF composite pellets sintered at 1200^0 C

In these XRD patterns, all the peaks are identified with either LSMO or CF without any impurity or secondary phases. LSMO phase has orthorhombic crystal structure whereas CF phase is cubic. The most intense peak of CF phase increases with addition of CF in the composites. To observe the peak shift of LSMO ($2\theta = 32.23$), slow scan of these composites are performed and XRD patterns are shown in Fig. 4.12. The structural transition from monoclinic (LSMO) to orthorhombic (LSMO) was also observed in this process. For 50LSMO: 50CF the

same peak shifts towards higher angle this implies there is a compression in the plane by changing the lattice parameter. This is may be due to the size factor (ionic radius of Sr^{+2}= 1.12 Å whereas ionic radius of Co^{+2}= 0.745 Å). The phase, lattice parameter and cell volume of these composites are given in Table 4.6.

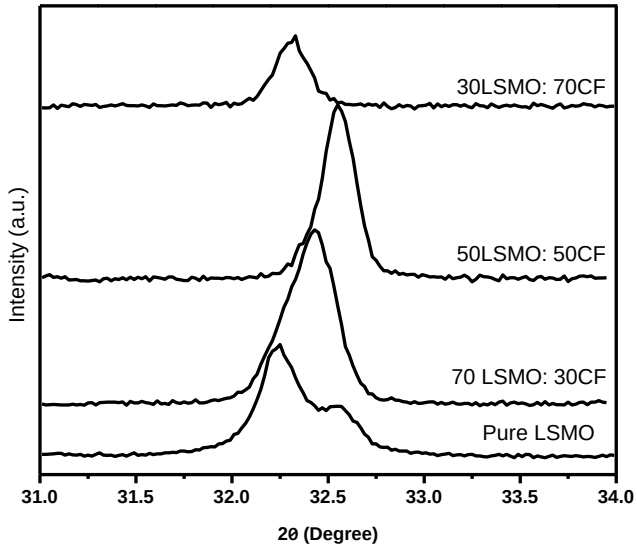

Fig. 4.12: Slow scan XRD patterns of LSMO in LSMO: CF composite

Table 4.6: Phase, lattice parameters and cell volume of LSMO: CF composites

(1-x)LSMO: x CF composite	Structure	Lattice parameter (Å)	Cell volume (A^3)
70LSMO:30CF	LSMO(O) CF (C)	a= 7.52 b= 8.73 c= 9.45 a=b=c= 8.39	620.38
50LSMO:50CF	LSMO(O) CF(C)	a= 7.20 b= 8.69 c= 9.33 a=b=c= 8.39	583.75
30LSMO:70CF	LSMO(O) CF (C)	a= 6.70 b= 8.61 c= 6.39 a=b=c= 8.39	368.61

Note: O represents orthorhombic structure of LSMO and C represents cubic structure of CF.

4.3.2 Microstructural and particle size distribution

Phase distribution and morphology were performed using back-scattered mode SEM on the sintered ball milled LSMO: CF composites. Fig. 4.22 (a), (b) and (c) shows the SEM micrographs along with EDAX as well as number of grains as a function of grain size (from SEM micrographs) for the composites 70 mol% LSMO: 30 mol% CF, 50 mol% LSMO: 50 mol% CF and 30 mol% LSMO: 70 mol% CF, respectively.

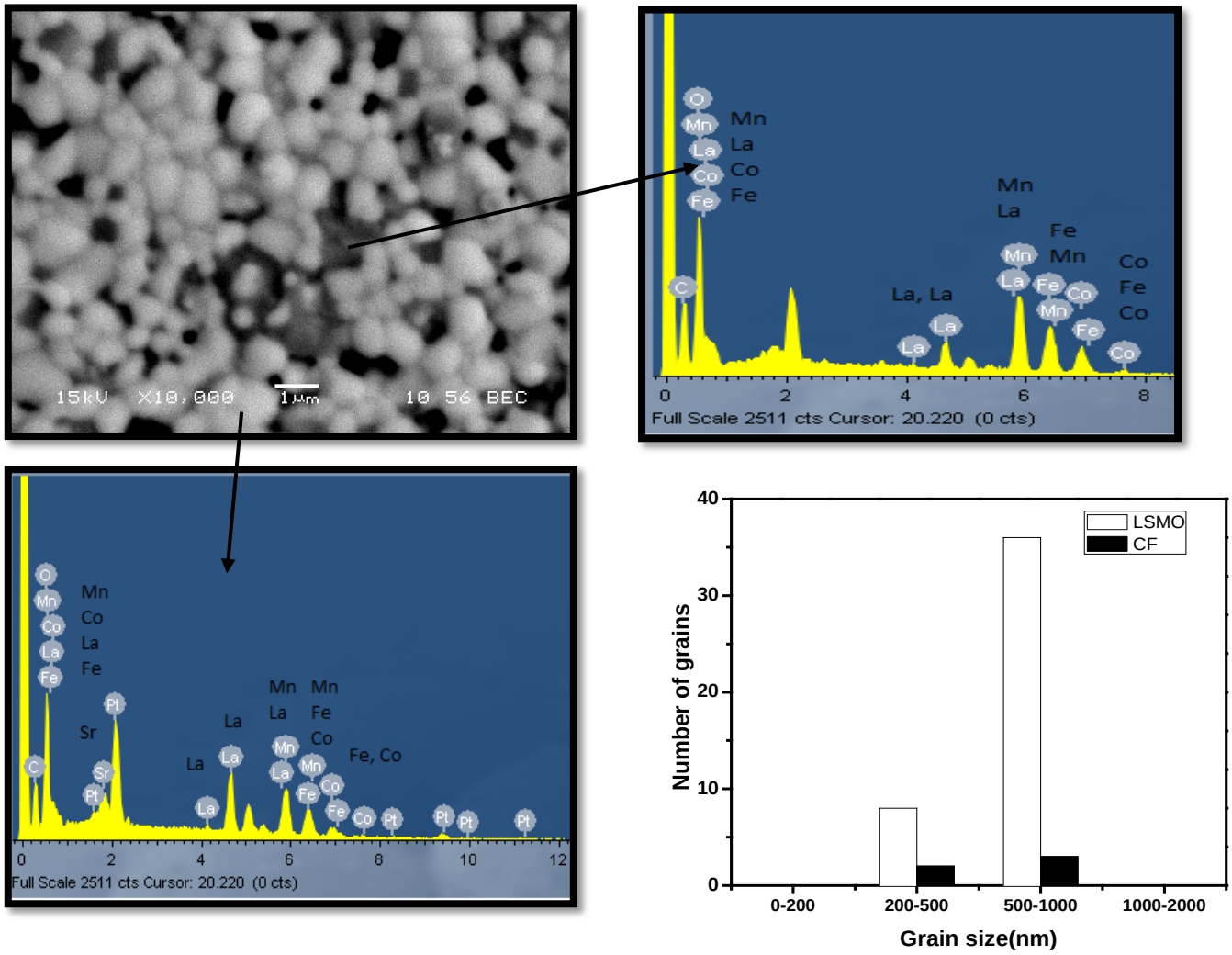

Fig. 4.13 (a): SEM micrograph, EDAX and number of grains as a function of grain size for 70 mol% LSMO: 30 mol% CF composites

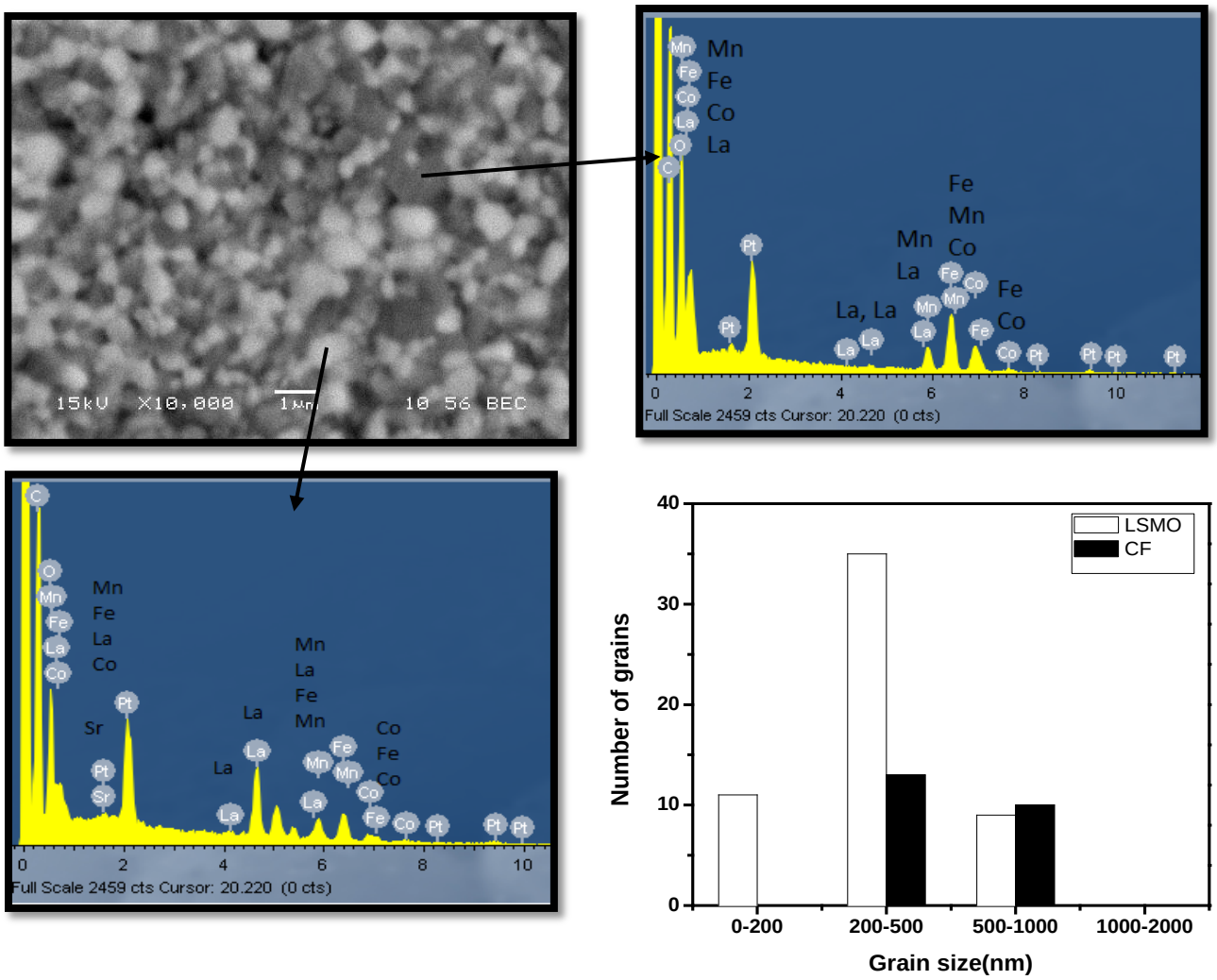

Fig. 4.13 (b): SEM micrograph, EDAX and number of grains as a function of grain size for 50 mol% LSMO: 50 mol% CF composites

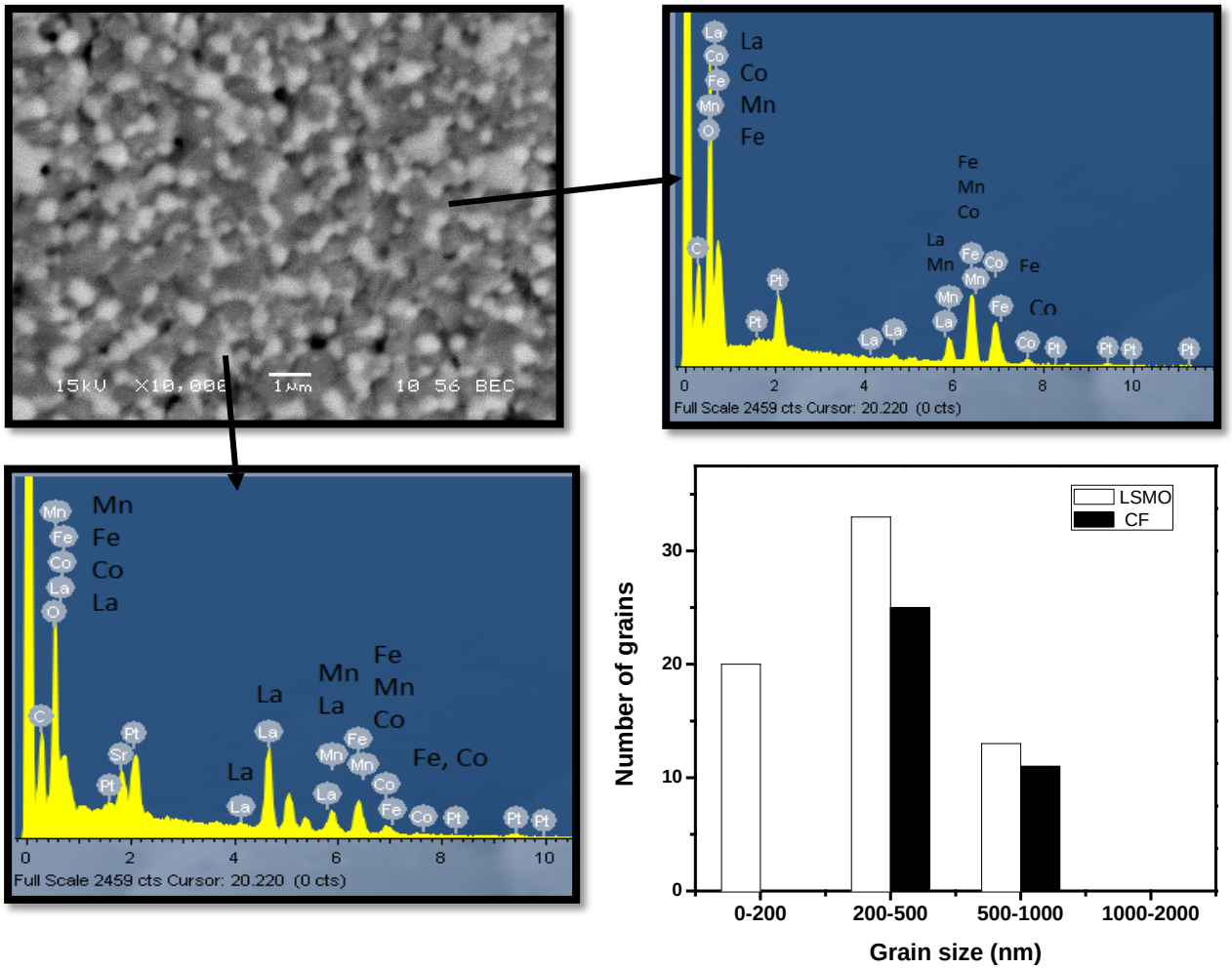

Fig. 4.13 (c): SEM micrograph, EDAX and number of grains as a function of grain size for 30 mol% LSMO: 70 mol% CF composites

After ball milled, the particle shape became nearly spherical with uniform size for all composites as seen from the SEM micrographs. In all microstructures, the white portions indicate the presence of LSMO phase and the black portion indicates the presence of CF phase, and also confirmed from EDAX analysis. The two phase system is clearly seen from SEM micrographs except for 70 mol % LSMO: 30 mol % CF composites. In this case, the LSMO grains are well surrounded by the thin layer of CF. The microstructure of 70 mol % LSMO: 30 mol % CF composite is totally different from other composites. From microstructures, it was also came to know that the maximum numbers of grains of 30 and 50 LSMO composites are in the range of 200-500 nm whereas 70 LSMO: 30CF composite is the range of 500-1000 nm.

Particle size distribution for all composites are done using particle size analyzer and the average particle size of these composite are found to be in the range between 200 nm to 300 nm. Particle size distribution of the 30LSMO:70 CF composite sintered at 1200^0C powder is shown in Fig. 4.14. It is also clear from the figure that particle size distribution for this composite is narrow in comparison that of the composite prepared by microwave refluxing synthesis technique.

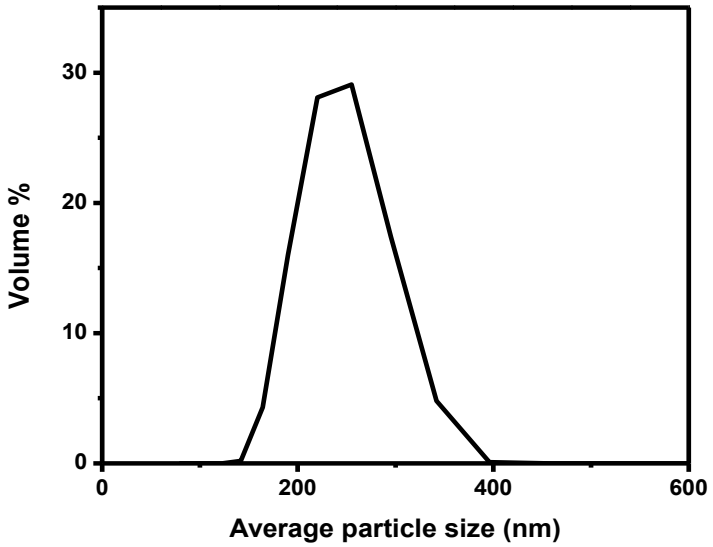

Fig. 4.14: Particle size distribution of 30LSMO: 70CF composite sintered at 1200^0C

The density of all sintered composites is given in Table 4.7. More than 94% density was observed for all composites due to its morphology. Density increases with increase in CF content and highest density was obtained for 70 and 30 mol % CF addition.

Table 4.7 density of pellets 30LSMO:70CF, 50LSMO:50CF, 70LSMO:30CF

LSMO: CF	Dry weight (gm)	Suspended weight (gm)	Soaked weight (gm)	Density
70:30	0.5718	0.4967	0.5796	98%
50:50	0.5588	0.4778	0.5639	94%
30:70	0.5581	0.4741	0.5631	97%

4.3.3.4 Magnetization

The magnetization as a function of field at a room temperature for all ball milled composites is shown in Fig. 4.15.

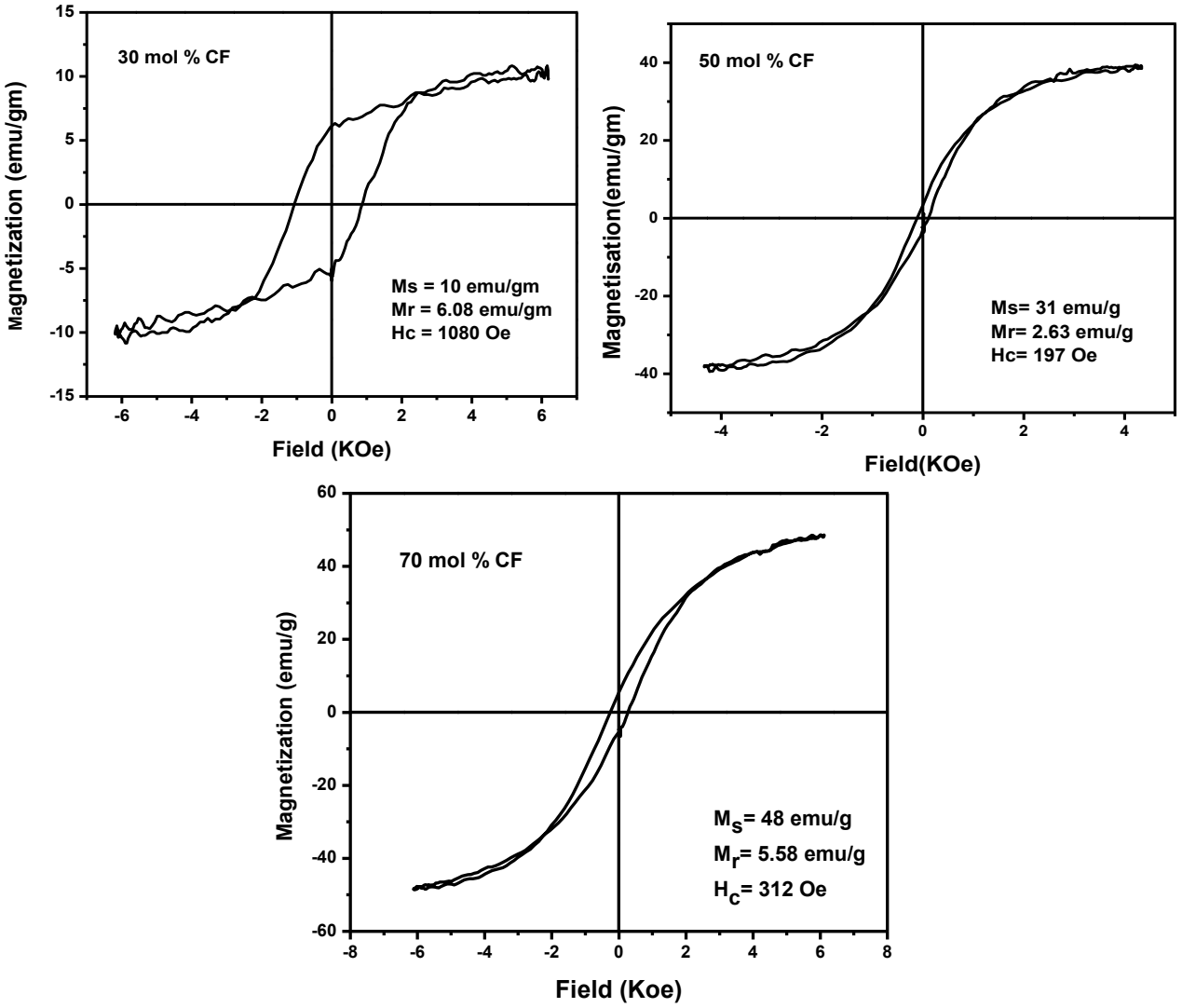

Fig. 4.15: Room temperature M-H loop of ball milled LSMO: CF composites

Tables 4.8 summarize the magnetic data of the LSMO: CF composite. Maximum coercivity of 1080 Oe was obtained from 30 mol % CF addition as compared to other composites which was strongly depends on the different morphology as compared to other composites. Due to thin layer of CF on LSMO grains for 70 mol % LSMO: 30 mol% CF composites, the pinning effect is more as compared to other composites.

Table 4.8 magnetic datas of the 30 and 70 LSMO: CF composites sintered at 1200^0C.

Samples	Coercivity Hc, (Oe)	Remanent magnetization M_r, (emu/gm)	Saturation magnetization M_s, (emu/gm)
70LSMO:30CF	1080	6.08	10
50LSMO:50CF	197	2.63	31
30LSMO:70CF	312	5.58	48

4.3.4 Summary

The microstructural and magnetic properties of ball milled LSMO: CF composites are different from the in-situ LSMO: CF composites. In XRD study, all the peaks are identified with either LSMO or CF without any impurity or secondary phases. The two phase system is clearly seen from SEM micrographs except for 70 mol % LSMO: 30 mol % CF composites (in this case, LSMO grains are well surrounded by the thin layer of CF). Maximum coercivity of 1080 Oe was obtained form 30 mol % CF composites due to different morphology which give more pinning effect.

Chapter – 5

Conclusions

5.1 Conclusions

The significant findings of this work are:

1. It is possible for successful preparation of composite material consisting of LSMO and CF by in-situ microwave refluxing and by ball mill. The applied synthesis route creates very significant effect on the microstructure and magnetic properties of the sample.
2. Sample prepared in basic medium have a stronger ferromagnetic in character. This suggests that the inversion of Fe ions is greater in the particles prepared in basic medium and also gives reduced grain size.
3. LSMO nanoparticles exhibit monoclinic to orthorhombic phase transition with increasing percentage of CF addition. This is may be due to the size factor (ionic radius of Sr^{+2}= 1.12 Å whereas ionic radius of Co^{+2}= 0.745 Å).
4. There is a variation in morphology, observed in the SEM micrographs of in-situ and ball milled samples.
5. The size of LSMO grains is smaller than CF grains.
6. M_s and H_c both are increased with increasing percentage of CF. presence of insulating phase forces the motion of electrons to move (bend) through the manganite grains, thereby increasing significantly the contribution of grain boundary to the conduction process. Since corecivity is a microstructural property, ball milled 70LSMO: 30CF composite gives higher corecivity. This may be due to its unique morphology as compared to other composites.

Chapter- 6

Future work

6.1 Future work

The present work leaves a wide scope for future investigators to explore many other aspects like its electric property, magnetoelectric effect at room temperature, colossal magnetoresistance (CMR) applications etc. The effect of internal strain on the magnetic property of this composite can also be studied.

Chapter- 7

References

7.1 REFERENCES

1. S. Asthana, A. K. Nigam and D. Bahadur, *Phys. Stat. Sol. B*, **243**, 1922–1928 (2006).
2. W.J. Lu, Y.P. Sun, X.B. Zhu, W.H. Song and J.J. Du, *Maters. Letters*, **60**, 3207 (2006).
3. S. Jin, T.H. Tietel, M. McCormack, R.A. Fastnacht, R. Ramesh and L.H.Chen, *Sci.*, **264**, 413 (1994).
4. M.B. Salamon and M. Jaime, *Rev. Mod. Phys*., **73**, 583 (2001).
5. S. Jin, T. Tiefel, M. McCormack, R. Fastnacht, R. Ramesh, and L. Chen, *Sci*., **264**, 413 (1994).
6. C.N.R. Rao, *Mater. Today*, 9- 13, (2006).
7. S. Das and T.K. Dey, *Solid State Commu*., **134,** 837 (2005).
8. C.N.R. Rao, *Mater. Today*, 9- 13, (2006).
9. C.Zener, *Phys. Rev*., **82**, 403, (1951).
10. M. Bowen, M. Bibes, A. Barthélé my, J.P. Contour, A. Anane and A. Fert, *Appl. Phys. Lett.*, **82** , 233, (2003).
11. R. Desfeux, S. Bailleul, A.D. Costa, W. Prellier and A.M. Haghiri-Gosnet, *Appl. Phys. Lett.*, **78**, 3681, (2001).
12. A. Hunyek**,** C. Sirisathitkul and P. Harding, *Adv. Mater. Research*, **93**, 659 (2010).
13. M.Barsoum, "*Fundamentals of ceramics*", IOP publishing, Bristol and Philadelphia, 584-586 (2003).
14. C. Barry Carter and M. Norton, "Ceramic materials: science and engineering", *Springer*, 101 (2007).
15. D. Shriver, P. Atkins, T. L. Overton, J. P Rourke, M. T Weller and F. A. Armstrong, "*Inorganic Chemistry*" W. H. Freeman, New York, (2006).
16. V. Pallai and D.O. Shah, *Jour. Magnetism Magnetic Materials*, **163,** 243-248 (1996).
17. R Skomski, *J. Phys. Condens. Mater*., **15**, R1-R56, 2003.
18. Y. Tokura, *Solid State Mater. Sci*., **3**, 175-180 (1998).
19. R. Müller, W. Schüppel, T. Eick, H. Steinmetz and E. Steinbeiß, *J. Magn. Magn. Mater*., **217**, 155 (2000).
20. R. W. Siegel, *Ann. Rev. Mater. Sci*., **21**, 559 (1991).
21. R. W. Siegel, *Nanostruc. Mater*., **3**, 1 (1993).
22. C. Liu, *J. Am. Chem. Soc*., **122**, 6263 (2000).

23. A.D. Andres, M. Garcıa-Hernandez and J.L. Martınez, *Phys. Rev. B*, **60**, 7328 (1999).
24. D. Das, A. Saha, S. E. Russek, R. Raj and D. Bahadur, *Jour. Appl. Phys*., **93**, 8301 (2003).
25. Y.Cedeno-Mattei and O.Perales-Perez, *Micro. Electro. Jour*., **40**, 673-676 (2009).
26. T. Tang, S. Y. Zhang, R. S. Huang, and Y. W. Du, *J. Alloys and Comp.*, **353**, 91 (2003).
27. J. Rivas, L. E. Hueso, A. Fondado, F. Rivadulla and M. A. López-Quintela, *J. Magn Magn. Mater.*, **221**, 57 (2000).
28. C.-H. Yan, Z.-G. Xu, T. Zhu, Z.-M. Wang, F.-X. Cheng, Y.-H. Huang, and C.-S. Liao, *J. Appl. Phys.*, **87**, 5588 (2000).
29. Z.F. Zi , Y.P. Sun, X.B. Zhu, C.Y. Hao, X. Luo, Z.R. Yang, J.M. Dai, W.H. Song, *Jour. Alloys Comp*., **477**, 414-419 (2009).
30. C.S. Xiong, F.F.Wei, Y.H. Xiong, L.J. Li, Z.M. Ren, X.C. Bao, Y. Zeng, Y.B. Pi, Y.P. Zhou, X.Wu and C.F. Zheng, *Jour. Alloys Comp*, **474** , 316-320 (2009).
31. C.H.Yan, Z.G.Xu, T.Zhu, Z.M.Wang, F.X.Cheng, Y.H.Huang and C.G.Liao, *Jour. Appl. Phys*., **87**, 5588 (2000).
32. Q. Huang, J. Li, X. Huang, C. K. Ong, and X. S. Gao, *J. Appl. Phys.*, **90**, 2924 (2001).
33. C. O. Kappe, *Angew. Chem. Int.* **43**, 6250 (2004).
34. S Das, A K Mukhopadhaya, S Datta and D Basu, *Mater. Sci*., **31**, 943–956 (2008).
35. S. Shi and J-Yang Hwang, *Jour. of Minerals Mater. Charac. Engg*., **2**, 102 (2003).
36. J. Giri, T. Sriharsha, S. Asthana, Tumkur K. Gundu Rao, Arun K. Nigam and D. Bahadur, *Jour. Magnetism Magnetic Mater*., **293**, 55-61 (2005).
37. A.K. Bose, B.K.Banik, N. Lavlinskaia, M. Jayaraman and M.S.Manhas, *Jour. Chem.Tech*., **27**, 18–24 (1997).
38. R.David and D.Michael, *Jour.Organometallic Chem*., **384**, C57-C60 (1990).
39. C. O. Kappe, D. Dallinger, and S. Shaun Murphree, *"Microwave synthesis – an introduction*, 42-48 (2005).
40. B. B. Nayak, S. Vitta and D. Bahadur, *Maters. Sci. Engg. B*, **139**, 171–176 (2007).
41. Q. Huang, J. Li, X. J. Huang, C. K. Ong and X. S. Gao, *Jour. Appl. Phys*., **90**, 2924-2929 (2001).
42. Y. P. Liu, Y. S. Du, M. Zhang, H. Yan and Y. Y. Wang, *Vacuum*, **81**, 826- 829 (2007).

43. Z. M. Tian, S. L. Yuan, Y. Q. Wang, L. Liu, S. Y. Yin, P. Li, K. L. Liu, J. H. He and L. Q. Li, *Mater. Sci. Engg. B*, **150**, 50-54 (2008).
44. Z. M. Tian, S. L. Yuan, Y. Q. Wang, L. Liu, S. Y. Yin, P. Li, K. L. Liu, J. H. He and J. Q. Li, *Mater. Sci. Engg. B*, **150**, 50-54 (2008).